# Automatic colorization with improved spatial coherence and boundary localization

Wei Zhang [1] Member, IEEE
Chao-Wei Fang [1]
Guan-Bin Li [2] * Member, IEEE

[1] *Department of Computer Science, the University of Hong Kong, Hong Kong, China*
[2] *School of Data and Computer Science, Sun Yat-Sen University, Guangzhou, Guangdong, China*

E-mail: wzhang2@cs.hku.hk; chwfang@connect.hku.hk; liguanbin@mail.sysu.edu.cn

Received submit date

**Abstract** Grayscale image colorization is an important computer graphics problem with a variety of applications. Recent fully automatic colorization methods have made impressive progress by formulating image colorization as a pixel-wise prediction task and utilizing deep convolutional neural networks. Though tremendous improvements have been made, it is still far from perfect. Specifically, there still exist common pitfalls in maintaining color consistency in homogeneous regions as well as precisely distinguishing colors near region boundaries. To tackle these problems, we propose a novel fully automatic colorization pipeline which involves a boundary-guided CRF and a CNN-based color transform as post-processing steps. In addition, as there usually exist multiple plausible colorization proposals for a single image, automatic evaluation for different colorization methods remains a challenging task. We further introduce two novel automatic evaluation schemes to efficiently assess colorization quality in terms of spatial coherence and localization. Comprehensive experiments demonstrate great quality improvement in results of our proposed colorization method under multiple evaluation metrics.

**Keywords** Automatic colorization, Deep learning, Conditional random field, Color transforms, Quality evaluation

## 1 Introduction

Image colorization aims to convert grayscale images to colorful ones. This task has attracted a lot of research in computer graphics due to its practical application values, such as colorizing old photographs and assisting creative works [1–15]. With user-assisted scribbles [1–5] or reference color images [7–14], traditional research mainly focuses on developing better colorization systems with less user interactions and time consumption. Interestingly, human can effortlessly judge suitable colors for different regions just by a quick glance of a grayscale image. In order to make this process possible for a colorization system, recent research focuses on fully-automatic colorization techniques. Ideally, an automatic colorization system takes grayscale images as input and generates visually plausible color versions directly. This problem can be readily formulated as a pixel-wise regression problem in computer version and the effectiveness has been proven by

* Corresponding author. This work was partially supported by Hong Kong Research Grants Council under General Research Funds (HKU17209714).

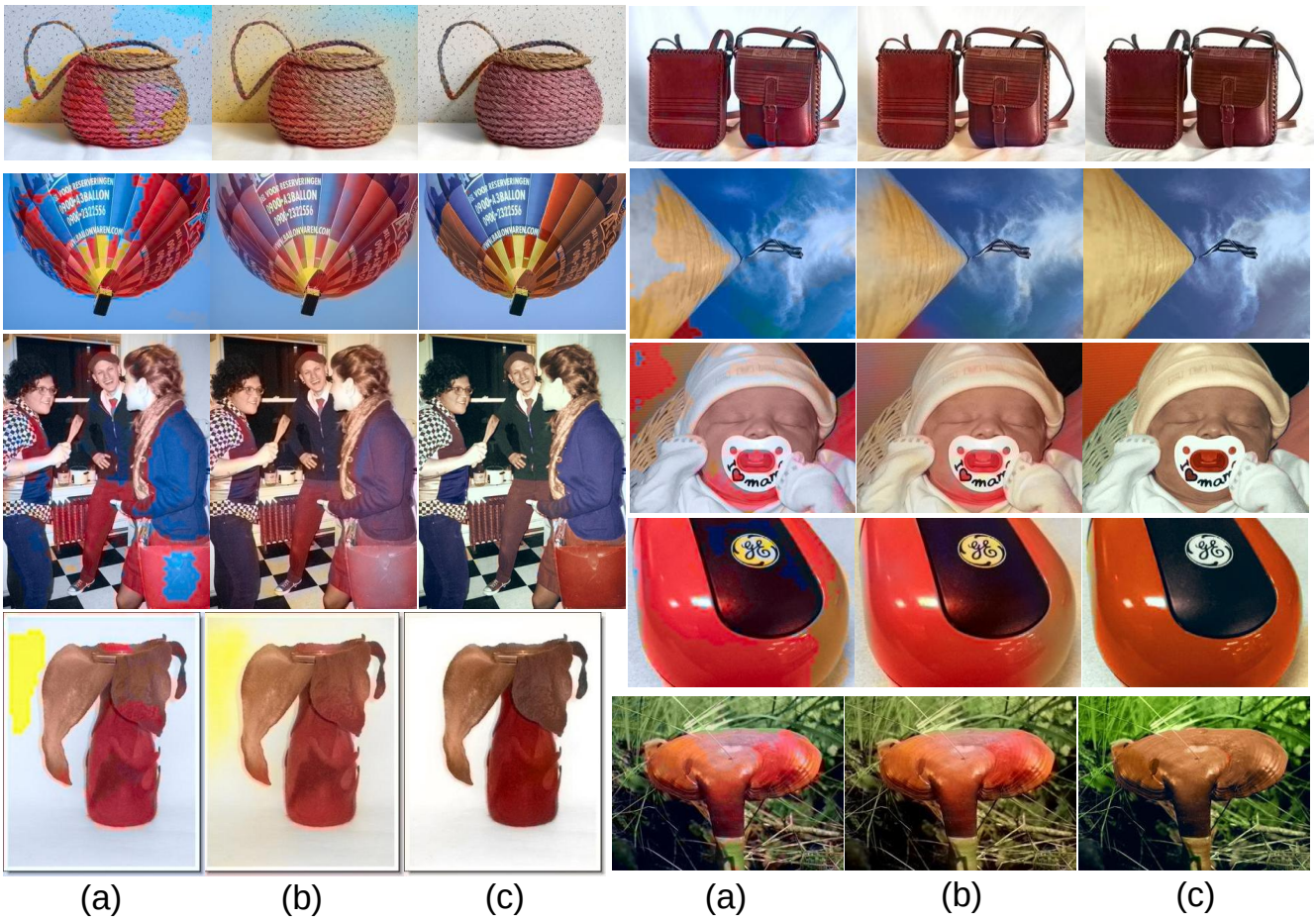


Fig. 1: Comparison with leading method proposed by Richard et al. [19]. In every set of three images, *(a):* Top-1 color prediction result by Richard et al. [19]; *(b):* Final result of Richard et al. [19] by calculating the expectation over color bins; *(c):* Our result which improves spatial consistency using CRF and chromatic resolution by color transform CNN.

Cheng et al. [16] and Dahl [17]. Over the past few months, Larsson et al. [18] and Richard et al. [19] both introduced classification based colorization frameworks built on deep convolutional neural networks (DCNNs). In order to produce colorization results with higher saturation and fidelity, they both learned pixel-wise labeling models over discrete color bins. Furthermore, Richard et al. [19] applied class re-balance during training and achieved state-of-the-art. Though significant improvement has been made in [18, 19], there are obvious drawbacks existing in maintaining color consistency in homogeneous regions as well as in precisely distinguishing colors near region boundaries. For example in Figure 1, in every set of three images, *(a)* shows the top-1 color predictions produced by [19]. Inconsistent color assignments can be commonly observed even in simple images with single object and uncomplicated background. Furthermore, poor localization of object boundaries often leads to color bleeding. Hence, even though the color prediction for major parts of image are correct, people can easily discover unreal colorization from such phenomena. Obviously, such existing shortages reveal that high quality automatic coloriztion remains a challenging task.

In this paper, we propose a novel pipeline which aims to improve the spatial coherence and boundary localization in colorization. Fully connected conditional random field (CRF) has been

widely used to improve the spatial accuracy in general DCNN based image labeling tasks, such as semantic segmentation, in which inputs are usually color images. However, colorization models only take grayscale images as input without any chromatic information, making it extremely hard to capture edge details and local consistency for a fully-connected CRF. To address this problem, we present a boundary-guided local CRF which is capable of improving pixel-wise color labeling results of DCNNs. Since the ultimate goal of colorization is to predict suitable color values for each pixel instead of fixed color category, one essential step at the end is to infer continuous values from labeling result. Current colorization system simply calculates the expectation [19] or takes the median value [18] over histogram bins. However, as shown in column *(b)* of Figure 1, such method brings no improvement but a blurry effect. In this paper, we introduce a color transform CNN to learn a better inference. As shown in column *(c)*, our final results achieve significantly improved quality both locally and globally.

We further introduce two novel evaluation schemes to automatically evaluate colorization quality in terms of regional consistency and boundary localization respectively on large datasets.

In summary, our contributions in this paper can be summarized as follows:

- We introduce a novel automatic colorization framework based on DCNN. With a boundary-guided local CRF and a color transform CNN as post-processing steps, our system is not only capable of capturing detailed edge information from grayscale images to facilitate better color labeling, but also learns a mapping from labeling results valued in fixed color bins to final color values;

- We develop two novel schemes for efficient quality evaluations through large numbers of automatic colorization results. Our proposed evaluation schemes reflect human's common preference for high quality colorizations. Experimental results illustrate our colorization method achieves much better performance than previous methods under both evaluation schemes.

## 2 Related work

We review recent automatic colorization systems and existing evaluation criteria in this section.

**Automatic colorization** Fully automatic colorization could be formulated as a pixel-wise prediction problem which is targeted at transforming one gray image to its color version. Cheng et al. [16] first attacked this problem by exploring a combination of different levels of handcrafted features for each pixel. They attempted to predict chromatic values using neural network with $L_2$ regression loss. Recently, end-to-end deep CNN features demonstrate considerably superior performance than traditional handcrafted ones in extensive vision tasks [20–26]. Hence it is not surprising with state-of-the-art deep CNN architectures, Dahl [17] obtained better results than [16] even though the loss function is still $L_2$ regression. Iizuka et al. [27] generated promising results on scene centered photographs through taking advantage of a two steam DCNN architecture where a joint training strategy is used to fuse scene classification cues. More recently, [18, 19] further address the underlying label uncertainty problem in automatic color prediction by formulating colorization as a pixel-wise labeling problem instead of regression. Typically, they first divided color space into discrete bins and then trained a DCNN to predict the probability distribution over bins. Their DCNN architectures are close in spirit: Larsson et al. [18] use hyper-columns [28] of multiple feature maps while Richard et al. [19] adopt dilated convolutions [29] and layer concatenation. In addition, Richard et al. [19] figure out the problem of extremely unbalanced distribution over color bins through introducing class-rebalancing during training which helps to boost the performance

to the state-of-the-art.

**Evaluation criterion** The ultimate goal of an automatic evaluation is to determine the consistency of the generated colorization results with human expectation. It's a non-trivial task specially because in most cases, there exist multiple reasonable color schemes which appear to be both realistic and vibrant for one grayscale image. Though each grayscale image in the testing set [18, 19] has corresponding color version as ground-truth, simply expecting exactly the same colorization results as ground-truth is overly strict. Here we summarise existing evaluation criteria for automatic colorization systems.

Direct pixel-wise comparison:

- **PSNR:** Peak signal-to-noise ratio in RGB color space. [16, 18]

- **RMSE** and **Raw Accuracy:** Root mean square error in ab color space over all pixels. [18, 19]

- **Rebalanced Raw Accuracy:** Re-weight the raw pixel distance inversely by color class probability . [19]

Semantic interpretability:

- **Image classification:** Feed automatically colorizated images and corresponding ground-truth images respectively to an off-the-shelf image classifier which is trained on real color images. Compare their results in classification accuracy. [19]

User-assisted evaluation:

- **Naturalness:** Users are asked to answer "Does this image look natural to you?" after observing each sample image within a limited time. [27]

- **Color Turing Test:** One real image and the recolorized counterpart are presented to participants together, then ask them to point out the fake one. [19]

Among existing evaluation criteria, evaluation methods based on direct pixel-wise comparison expect same color values as ground-truth thus they are overly strict. Moreover, it's hard to prove the consistency between image classification accuracy and colorization quality. User involved studies directly reflect human's observation but are too costly when dealing with large datasets. As far as we know, no existing criterion has taken into consideration common artifacts like regional inconsistency and color bleeding which are widespread in current colorization models. To address these limitations, we propose two novel evaluation schemes which consider regional inconsistency and color bleeding artifacts into quality evaluation of colorization.

## 3 Algorithm

Our full pipeline can be formulated as a function $F$, which maps a single channel input image $\boldsymbol{X} \in \mathbb{R}^{H\times W\times 1}$ to two color channels $ab$ $\widehat{\boldsymbol{Y}} \in \mathbb{R}^{H\times W\times 2}$ in CIE$Lab$ color space, where $H, W$ are spatial dimensions:

$$\widehat{\boldsymbol{Y}} = F(\boldsymbol{X}).$$

Denote $\boldsymbol{Y}$ as the $ab$ channels of the ground-truth color image. $\widehat{\boldsymbol{Y}}$ is expected to be close to $\boldsymbol{Y}$ during the learning procedure. The overview of the proposed pipeline is illustrated in Figure 2. It consists of three main phases: an initial colorization model, boundary-guided conditional random field (CRF) and a color transform convolutional neural network (CNN). Firstly, the target grayscale image is fed to a classification based colorization model which generates a probability distribution over discrete color bins for each pixel. Secondly, we calculate the unary term of CRF based on the predicted probability distribution. When calculating the pairwise affinity of CRF, we involve boundary cues which are obtained by an off-the-shelf boundary detector from input grayscale image. With such boundary-guided CRF, we aim to improve the spatial coherence of the initial labeling result. Subsequently, to infer final continuous color values, we adopt a CNN to learn a transformation from discrete color bins to continuous color values. In the reminder of this section, we will elaborate three phases sequentially.

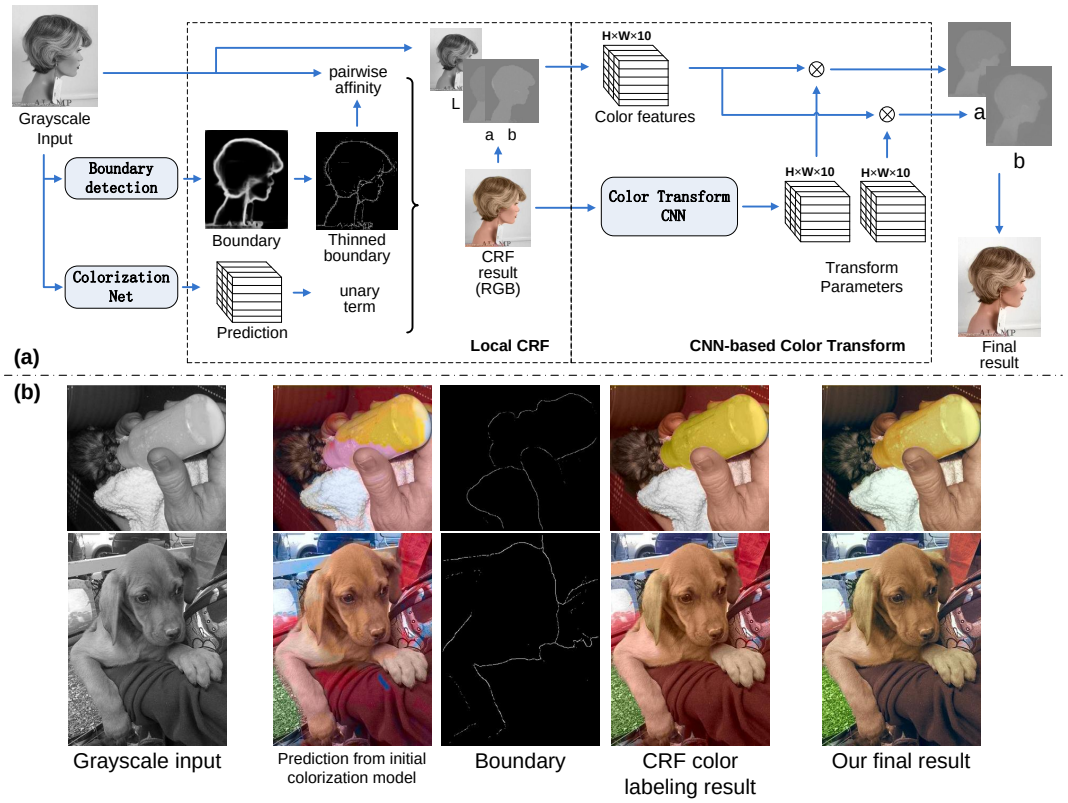


Fig. 2: *(a):* Overview of our full pipeline for automatic colorization. *(b):* Example images of each phase in our pipeline.

### 3.1 Initial colorization

To obtain a good initial prediction result over color bins, we adopt a state-of-the-art deep colorization CNN [19] as our initial colorization model. Following [19], we divide $ab$ two dimensional plane into $Q = 313$ bins and learn a pixel-wise classification model from input grayscale image via deep CNN in an end-to-end manner:

$$\widehat{\boldsymbol{P}} = G(\boldsymbol{X})$$

where $G$ denotes the deep CNN and $\widehat{\boldsymbol{P}} \in [0,1]^{H\times W\times Q}$ represents the predicted probability distribution over color bins. Unlike in [19] where the expectations over color bins are calculated as the final color values, we further adopt a boundary-guided CRF to improve spatial coherence in labeling result.

### 3.2 Boundary-guided CRF

Let $\phi(i)$ be the expected color label for pixel $p_i$, and $\widehat{P}_{i,\phi(i)}$ be the probability of assigning color label $\phi(i)$ to pixel $p_i$. $\widehat{P}_{i,\phi(i)}$ can be predicted by the initial colorization DCNN. The standard energy function of local CRF is defined as follows.

$$E(\phi) = E_{unary} + \gamma E_{pair}, \tag{1}$$

$$where \quad E_{unary} = -\sum_i \log \widehat{P}_{i,\phi(i)}, \tag{2}$$

$$E_{pair} = \sum_i \sum_{p_j \in N_{h(p_i)}} \omega_{ij}\tau(\phi(i),\phi(j)), \tag{3}$$

$$where \quad \omega_{ij} = \exp\left(-\frac{\|\boldsymbol{f}_i - \boldsymbol{f}_j\|_2^2}{2\sigma^2}\right), \tag{4}$$

$$\tau(\phi(i),\phi(j)) = \begin{cases} 1, \phi(i) \neq \phi(j); \\ 0, otherwise, \end{cases} \tag{5}$$

where $N_{h(p_i)}$ is a $h \times h$ neighborhood centered at pixel $p_i$, and $\boldsymbol{f}_i$ represents the feature of pixel $p_i$ in the target image.

The unary term in Eq.2 is calculated based on $\widehat{P}_{i,\phi(i)}$ while the pairwise term in Eq.3 models the spatial coherence of current labeling scheme, which is conventionally measured by the similarity between neighboring pixels. By this probabilistic graphical model, it is much desired to suppress artifact color predictions in homogeneous regions and keep color boundaries aligned with intrinsic changes perceived from grayscale input. However, due to the lack of chromatic values, $\boldsymbol{f}_i$ and $\boldsymbol{f}_j$ become scalars thus the distance space of $\boldsymbol{f}_i$ and $\boldsymbol{f}_j$ is seriously compressed compared with that in color images. This significantly increases the difficulty in discovering detailed edges from an image with only one gray channel. With this consideration, we modify conventional pairwise affinity in Eq.4 to Eq.6 to explicitly involve boundary cues:

$$\omega_{ij} = min\left(\exp\left(-\frac{\|\boldsymbol{f}_i - \boldsymbol{f}_j\|_2^2}{2\sigma^2}\right), (1-\hat{g}_{ij})^{\rho}\right) \tag{6}$$

where $\rho$ is a constant and $\hat{g}_{ij}$ represents the maximum boundary response value along the line segment between pixels $p_i$ and $p_j$. To obtain salient boundaries in grayscale images, we fine-tune the model of state-of-the-art boundary detector HED [26] using gray scale images and adopt an edge-thinning operation.

$$\tau(\phi(i), \phi(j)) = \|\phi(i) - \phi(j)\|_2^2 \tag{7}$$

Furthermore, since class labels are coordinates in a two-dimensional space spanned by $a, b$ chromatic channels, we model the relation between different labels using the Euclidean distance shown in Eq.7 instead of Eq.5. We obtain the color labeling results by minimizing the energy function in Eq.1 using graphcuts [30]. In our implementation, we set $\lambda = 0.5$ and $\rho = 10$.

### 3.3 CNN-based color transform

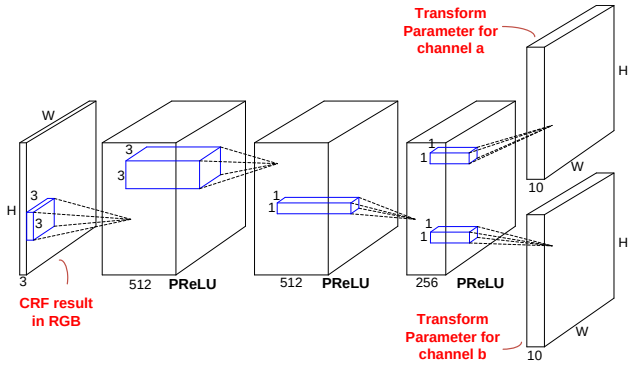


Fig. 3: Architecture of color transform CNN.

As aforementioned, color labeling should not be treated as the final result for colorization due to the fact that realistic color images are composed of large variety of color values in nearly continuous space. Thus inferring continuous values from CRF labeling results is important for final colorization quality. In this section, we introduce a CNN-based color transform model accounting for final color inference.

As shown in the last phase in Figure 2, proposed color transform model takes CRF result images in RGB color space as input and outputs two transform parameter cubes for $a, b$ chromatic channels respectively. Compared with deep colorization network which consists of 22 convolutional layers, our proposed color transform CNN only requires 4 convolutional hidden layers which slightly increases the computational complexity but gains obviously better color inference results than previous methods. The detailed architecture of proposed color transform CNN is shown in Figure 3 and Table 1. Specifically, first 3 hidden layers are shared while the last layer contains two separate branches for learning transform parameter cubes of $a, b$ color channel respectively. We adopt the Parametric Rectified Linear Unit (PReLU) [31] as the non-linear activation function between convolutional layers.

Let $\Phi$ be the color transform CNN. Let $\mathcal{I}_{rgb}$ and $\mathcal{I}_{Lab}$ represent the initial colorized image


Fig. 4: Colorization results with and without CNN-based color transform. *(a):* Color labeling results from CRF. *(b):* Colorization results from color transform CNN.

outputted by boundary-guided CRF in RGB and CIE$Lab$ color space respectively. We use $\boldsymbol{U}$ to denote the feature extracted from $\mathcal{I}_{Lab}$, in which a quadratic color feature $[l^2, a^2, b^2, l*a, l*b, a*b, l, a, b, 1]^T$ is calculated for each pixel. Therefore, $\boldsymbol{U}$ is a $H \times W \times 10$ dimensional feature cube, where $H, W$ are spatial dimensions of $\mathcal{I}_{Lab}$. The proposed color transform CNN can be formulated as:

$$\boldsymbol{Q}^a = \Phi(\{\Theta_1, \Theta_2, \Theta_a\}, \mathcal{I}_{rgb})$$
$$\boldsymbol{Q}^b = \Phi(\{\Theta_1, \Theta_2, \Theta_b\}, \mathcal{I}_{rgb})$$

where $\boldsymbol{Q}^a$ and $\boldsymbol{Q}^b$ are $H \times W \times 10$ dimensional color transform parameter cubes for channel $a, b$ respectively. $\Theta_1$, $\Theta_2$ represent the weights of first two convolutional layers while $\Theta_a$, $\Theta_b$ are the weights of last layer for channel $a, b$ respectively.

The loss function is defined as follow:

$$L = \frac{1}{2}\sum_{i}^{H}\sum_{j}^{W}[(\sum_{k=1}^{10}\boldsymbol{Q}^a_{i,j,k}\boldsymbol{U}_{i,j,k} - \boldsymbol{Y}^a_{i,j})^2 + (\sum_{k=1}^{10}\boldsymbol{Q}^b_{i,j,k}\boldsymbol{U}_{i,j,k} - \boldsymbol{Y}^b_{i,j})^2]$$

where $\boldsymbol{Y}^a$ and $\boldsymbol{Y}^b$ represent $a, b$ channels of ground-truth color image respectively. We implement this color transform CNN based on the popular open source framework Caffe [32] and solve the energy minimization using standard stochastic gradient descent with learning rate 0.001 and weight decay 0.0005;

| Layer | Kernel | Stride | Dilation | Outputs |
|---|---|---|---|---|
| data | | | | 3 |
| conv1 | 3 | 1 | 1 | 512 |
| conv2 | 3 | 1 | 1 | 512 |
| conv3 | 1 | 1 | 1 | 256 |
| conv4_a/b | 1 | 1 | 1 | 10 |

**Table** 1: Color transform CNN architecture.

Figure 4 shows examples of our colorization results with or without applying CNN-based color transform. The comparison shows CNN-based color transform infers continuous chromatic values from discrete labeling results without significantly shifting color values, making our final colorization more natural and realistic.

## 4 Spatial-consistency evaluation

In this section, we introduce two novel evaluation schemes to efficiently measure color consis-

tency and boundary contrast consistency in generated colorful images.

### 4.1 Regional color consistency

Regional color consistency is one of the key factors for plausible colorization results. In real color images, different levels of chromatic variations can be observed in variant semantic regions: some regions are visually homogeneous while others may contain textures or be photographed under complex lighting environment. Though not knowing about the ground-truth, people can effortlessly judge unreal colorization once capturing inconsistent colors in homogeneous regions. Such observation indicates that measuring color variations in homogeneous regions is a promising strategy for evaluating colorization quality. Based on this, we propose to evaluate colorization quality by sampling a pixel group in each homogeneous region then calculating its color variation.

One example of the proposed evaluation scheme is shown in Figure 5. For each testing image, the ground-truth color version is transformed to CIE$Lab$ color space, in which $L$ dimension represents lightness and $a, b$ represent color-opponent dimensions. We first perform graph based segmentation [33] to generate superpixels. Note that in order to weaken the interference of lightness variations, graph based segmentation is operated on pixelwise color vectors $\boldsymbol{f}_c = [k*l, a, b]^T$ where $k$ is used for controling the weakening degree of $L$ channel. We collect one representative pixel which is spatially closest to its centroid, from each superpixel. Due to large color variation in the whole image, it is unreasonable to directly calculate color consistency over all representative pixels. Thus, we merely evaluate on pixel groups which locate in homogeneous regions.


Fig. 5: One example of color consistency evaluation. *(a):* Ground-truth color image; *(b):* Superpixels generated by graph based segmentation on pixelwise color vectors $\boldsymbol{f}_c = [k * l, a, b]^T$ (shown in random colors); *(c):* Hierarchical image segmentation results (shown in random colors); *(d):* Selected point group for consistency evaluation (shown in blue asterisks); *(e):* State-of-the-art colorization result by [19], $\widehat{\sigma}^r = 7.91$; *(f):* Our result, $\widehat{\sigma}^r = 1.43$.

Subsequently, we perform a fast hierarchical segmentation using MCG [34] to each ground-truth image and discard small segments which are below the average spatial size. In each remaining segment, we select one group from representative pixels with identical color value that is closest to the mean value of this segment in $ab$ channels. We further discard pixel groups which contain fewer than $S_r$ pixels. Finally, repeat the same selection scheme for all testing images, thus obtaining all pixel groups.

We denote the $i$th pixel group in image $j$ as

$G_{ij}$. Our regional color consistency evaluation is defined as follow:

$$W_r = \frac{1}{M}\sum_{j=1}^{M}\frac{1}{N_j}\sum_{i=1}^{N_j}\widehat{\sigma}^r_{i,j},$$
$$\widehat{\sigma}^r_{i,j} = \widehat{\sigma}_{a,i,j} + \widehat{\sigma}_{b,i,j}$$
$$where \quad \widehat{\sigma}_{c,i,j} = \sqrt{\frac{1}{P_{i,j}}\sum_{p_l \in G_{ij}}(\widehat{c}_{p_l} - \widehat{\mu}_{c,i,j})^2},$$
$$\widehat{\mu}_{c,i,j} = \frac{1}{P_{i,j}}\sum_{p_l \in G_{ij}}\widehat{c}_{p_l}, \quad c \in \{a, b\}$$

where $\widehat{\sigma}_{c,i,j}$ denotes the standard deviation of pixel group $G_{ij}$ in channel $a$ (or $b$) in the generated colorization image $j$. $P_{i,j}$ denotes the pixel number in group $G_{ij}$ and $\widehat{c}_{p_l}$ is the color value of pixel $p_l$ in a (or $b$) channel. $M$ is the number of total testing images and $N_j$ is the number of pixel groups in image $j$. We use $k = 0.3$ and $S_r = 10$ in our evaluation.

### 4.2 Boundary localization

Poor color discrimination along boundaries is another key factor which leads to the unreality of the generated colorization results. For example, image *(c)* in Figure 6 shows the generated colorization result of [19]. This model predicts suitable color for dog, sofa and carpet respectively but color bleeding across boundaries can be observed, e.g. colors for the dog bleeds over its boundary. Hence, we propose another approach to evaluate colorization quality in terms of boundary localization.

Figure 6 illustrates one example of our boundary localization evaluation scheme. For each ground-truth color image, we obtain its boundary map via HED [26] boundary detector, then threshold the resulted boundary map by 0.5 followed by an edge thinning operation. We subsequently divide boundaries into short sections using a boundary subdivision method [34] which involves a recursive boundary breaking procedure. Among the results, boundary sections with less than $S_b$ pixels are not considered. Afterwards, for each pixel located on resulted boundary sections, we sample $r$ pixels along the local boundary normal on both sides. In this way, two pixel groups are sampled on both sides of each selected boundary section. We calculate the variation of the $i$-th boundary section as bellow,

$$\sigma_{L,i} = \sigma_{L,i,a} + \sigma_{L,i,b}$$
$$\sigma_{R,i} = \sigma_{R,i,a} + \sigma_{R,i,b}$$
$$\sigma_i = \sigma_{L,i} + \sigma_{R,i}$$

where $\sigma_{L,i}$ and $\sigma_{R,i}$ represent the stand deviation of selected pixel group from left and right hand side of boundary section $i$. The subscript $a, b$ denote color channels in Lab color space respectively. We further filter out boundary sections with large variations by setting a low threshold $T_{std}$ for $\sigma_i$. Resulted boundary sections and sampled pixel groups on both sides provide the target locations for evaluation.

Finally, we define a localization evaluation criterion by calculating the color variation in colorized images according to target evaluation locations:

$$W_b = \frac{1}{M}\sum_{j=1}^{M}\frac{1}{N_j}\sum_{i=1}^{N_j}\widehat{\sigma}_{i,j}$$

where $N_j$ denotes the number of boundary sections selected in image $j$ and $M$ denotes the number of images for evaluation. We set $S_b = 10$ , $r = 10$ and $T_{std} = 50$ in our evaluation.

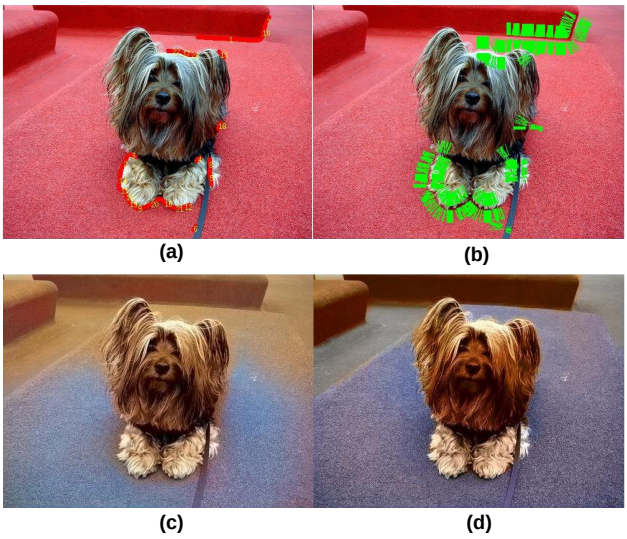


Fig. 6: One example of color bleeding evaluation. *(a):* Selected boundary sections for evaluation from ground-truth color image; *(b):* Selected pixel groups (shown in green color) on both sides of boundaries; *(c):* state-of-the-art colorization result by [19]; *(d):* Our result.

## 5 Experimental results

### 5.1 Experimental settings

We use the same dataset as in [19]: all the training images (around 1.3M) in ImageNet [35] are used as our training data, while the first 2k and last 10k images in the validation set of ImageNet are used as validation and testing data respectively in our experiments. For each testing image, it takes around 5 seconds to calculate the CRF labeling result and less than 1 seconds for all remaining steps in our proposed pipeline using a Nvidia Titan X GPU.

Since single evaluation criterion is not adequate for a comprehensive measurement of the colorization quality, we use multiple criterions to draw an overview of colorization results. Besides the proposed evaluation methods for color consistency and color bleeding, we further adopt the raw accuracy measure method [19] to provide a pixel-wise comparison with the corresponding ground-truth color images.

### 5.2 Raw accuracy evaluation results

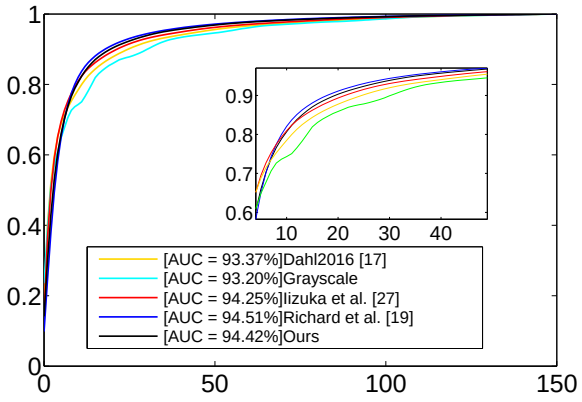


Fig. 7: Compare rebalanced Euclidean distance in ab color channels. A sub-figure that locates in the up-right corner shows the enlarged curve.

We employ the rebalanced variant of the AuC (area under curve) CMF (conditional mass function) metric [19] for a raw accuracy evaluation. This measurement first calculates the rebalanced pixel-wise Euclidean distance in $ab$ color channels between colorized image and its corresponding ground-truth color image. Then the curve is formed by calculating the percentage of pixels within certain distance from 0 to 150. Hence, higher AuC score indicates smaller distance between colorization results and ground-truths. The evaluation results are shown in Figure 7. As shown in Figure 7, except [17] and grayscale images, the AUC score of all the other three methods(including ours) are almost equal, with variation within 0.5%. So we conclude that regional color inconsistency and color bleeding phenomena, which apparently bring great visual defect, can not be reflected under the AuC metric. A visual comparison is demonstrated in Figure 9 and 10.

### 5.3 Consistency evaluation results

Following the proposed point group selection scheme introduced in section 4.1, 5525 images are selected from testing images for evaluation. Then

our proposed color consistency measurement is performed on locations of selected pixel groups in each testing image.

| Name | $W_r$ |
|---|---|
| Dahl [17] | 3.71 |
| Iizuka et al. [27] | 3.16 |
| Richard et al. [19] | 6.54 |
| Ours without color transform | 2.84 |
| Ours full pipeline | **2.63** |

**Table** 2: Color consistency evaluation results.

Table 2 lists the evaluation results using proposed criterion. As shown in the table, our colorization results significantly achieve the lowest color variations in homogeneous regions when compared with other leading colorization methods. Besides, we observe that the CNN-based color transform slightly improves the regional color consistency, although it is not initially designed for this purpose. This can be understood from the additional spatial smoothness that CNN-based color transform introduces.

### 5.4 Boundary localization evaluation results

Based on the proposed selection criterion introduced in section 4.2, 21156 boundary sections are selected for our color bleeding evaluation. The results of quantitative measurement on the selected boundary sections is illustrated in Table 3.

| Name | $W_b$ |
|---|---|
| Dahl [17] | 5.20 |
| Iizuka et al. [27] | 5.50 |
| Richard et al. [19] | 8.57 |
| Ours without color transform | 5.33 |
| Ours full pipeline | **5.16** |

**Table** 3: Boundary localization evaluation results.

Table 3 reveals that our colorization results give rise to much smaller chromatic variations on both sides of selected boundary sections. Meanwhile, we also observe CNN-based color transform slightly benefits boundary localiztion.

In general, our method achieves significant improvement in colorization quality by enhancing regional color consistency and eliminating color bleeding.

### 5.5 User study

In order to evaluate the colorization results quantitatively, we perform a user study. The user study is conducted by showing a pair of colorized images at a time, which are generated from one grayscale image using our proposed method and Richard et al. [19] respectively. The user is asked to choose *"Which image looks more natural to you?"* after comparing the two results. Unlike the user studies in Richard et al. [19] and Iizuka et al. [27], which only allow users to take a quick glance of each image pairs, we do not limit the time for each comparison and encourage users to combine their gut feeling with detailed observations. Besides, we provide a third option "Hard to decide" for each comparison in case users could not decide their preference. We invite 16 different participants in our user study, each shown 40 pairs of different images. All images are randomly chosen from testing dataset and randomly shown on the left or right hand-side to avoid bias.

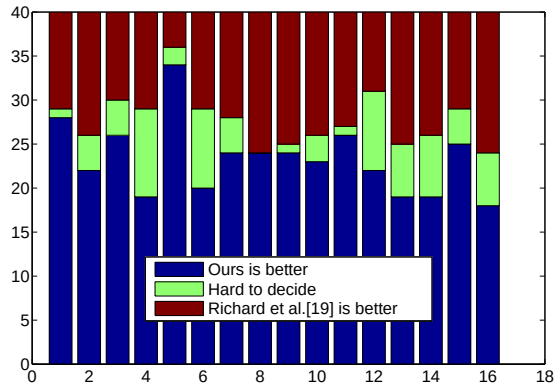


Fig. 8: Results of user study. We compare our method and a state-of-the-art method from Richard et al. [19] in terms of naturalness. The X-axis is the user ID while the Y-axis is the number of image pairs.

Figure 8 shows the result of the user study. We can see our method receives more user's satisfaction than state-of-the-art colorization method. Besides, during our user study, several participants mention that they clearly decide their preference by capturing the color bleeding phenomena, which is consistent with our proposed evaluation schemes.

## 6 Conclusion

In this paper, we propose post-processing steps for automatic image colorization, which involve a boundary-guided CRF and a CNN-based color transform model. Extensive experimental results demonstrate that our proposed methods greatly improve the colorization quality comparing with current leading methods. To prove the effectiveness of our proposed methods, we further introduce two novel evaluation schemes to quantitatively measure the quality of automatically colorized images in terms of color consistency and boundary localization.

## Acknowledgement

This work was partially supported by Hong Kong Research Grants Council under General Research Funds (HKU17209714).

## References

[1] Levin A, Lischinski D, Weiss Y. Colorization using optimization. In *ACM Transactions on Graphics (TOG)*, volume 23, 2004, pp. 689–694.

[2] Huang Y C, Tung Y S, Chen J C, Wang S W, Wu J L. An adaptive edge detection based colorization algorithm and its applications. In *Proceedings of the 13th annual ACM international conference on Multimedia*, 2005, pp. 351–354.

[3] Luan Q, Wen F, Cohen-Or D, Liang L, Xu Y Q, Shum H Y. Natural image colorization. In *Proceedings of the 18th Eurographics conference on Rendering Techniques*, 2007, pp. 309–320.

[4] Qu Y, Wong T T, Heng P A. Manga colorization. In *ACM Transactions on Graphics (TOG)*, volume 25, 2006, pp. 1214–1220.

[5] Zhao H L, Nie G Z, Li X J, Jin X G, Pan Z G. Structure-aware nonlocal optimization framework for image colorization. *Journal of Computer Science and Technology*, 2015, 30(3):478–488.

[6] Sheng B, Sun H, Magnor M, Li P. Video colorization using parallel optimization in feature space. *IEEE Transactions on Circuits and Systems for Video Technology*, 2014, 24(3):407–417.

[7] Welsh T, Ashikhmin M, Mueller K. Transferring color to greyscale images. In *ACM Transactions on Graphics (TOG)*, volume 21, 2002, pp. 277–280.

[8] Irony R, Cohen-Or D, Lischinski D. Colorization by example. In *Eurographics Symp. on Rendering*, volume 2, 2005.

[9] Charpiat G, Hofmann M, Schölkopf B. Automatic image colorization via multimodal predictions. In *European conference on computer vision*, 2008, pp. 126–139.

[10] Liu X, Wan L, Qu Y, Wong T T, Lin S, Leung C S, Heng P A. Intrinsic colorization. *ACM Transactions on Graphics (TOG)*, 2008, 27(5):152.

[11] Gupta R K, Chia A Y S, Rajan D, Ng E S, Zhiyong H. Image colorization using similar images. In *Proceedings of the 20th ACM international conference on Multimedia*, 2012, pp. 369–378.

[12] Jin S Y, Choi H J, Tai Y W. A randomized algorithm for natural object colorization. In *Computer Graphics Forum*, volume 33, 2014, pp. 205–214.

[13] Chia A Y S, Zhuo S, Gupta R K, Tai Y W, Cho S Y, Tan P, Lin S. Semantic colorization with internet images. In *ACM Transactions on Graphics (TOG)*, volume 30, 2011, p. 156.

[14] Deshpande A, Rock J, Forsyth D. Learning large-scale automatic image colorization. In *Proceedings of the IEEE International Conference on Computer Vision*, 2015, pp. 567–575.

[15] Li X, Zhao H, Nie G, Huang H. Image recoloring using geodesic distance based color harmonization. *Computational Visual Media*, 2015, 1(2):143–155.

[16] Cheng Z, Yang Q, Sheng B. Deep colorization. In *Proceedings of the IEEE International Conference on Computer Vision*, 2015, pp. 415–423.

[17] Dahl R. Automatic colorization. *http://tinyclouds.org/colorize/.*, 2016.

[18] Larsson G, Maire M, Shakhnarovich G. Learning representations for automatic colorization. *arXiv preprint arXiv:1603.06668*, 2016.

[19] Zhang R, Isola P, Efros A A. Colorful image colorization. *arXiv preprint arXiv:1603.08511*, 2016.

[20] Simonyan K, Zisserman A. Very deep convolutional networks for large-scale image recognition. *arXiv preprint arXiv:1409.1556*, 2014.

[21] Hariharan B, Arbeláez P, Girshick R, Malik J. Hypercolumns for object segmentation and fine-grained localization. In *Proceedings of the IEEE Conference on Computer Vision and Pattern Recognition*, 2015, pp. 447–456.

[22] Noh H, Hong S, Han B. Learning deconvolution network for semantic segmentation. In *Proceedings of the IEEE International Conference on Computer Vision*, 2015, pp. 1520–1528.

[23] Li G, Yu Y. Deep contrast learning for salient object detection. *arXiv preprint arXiv:1603.01976*, 2016.

[24] Li G, Yu Y. Visual saliency based on multiscale deep features. In *Proceedings of the IEEE Conference on Computer Vision and Pattern Recognition*, 2015, pp. 5455–5463.

[25] Ren S, He K, Girshick R, Sun J. Faster r-cnn: Towards real-time object detection with region proposal networks. In *Advances in neural information processing systems*, 2015, pp. 91–99.

[26] Xie S, Tu Z. Holistically-nested edge detection. In *Proceedings of the IEEE International Conference on Computer Vision*, 2015, pp. 1395–1403.

[27] Iizuka S, Simo-Serra E, Ishikawa H. Let there be color!: joint end-to-end learning of global and local image priors for automatic image colorization with simultaneous classification. *ACM Transactions on Graphics (TOG)*, 2016, 35(4):110.

[28] Noh H, Hong S, Han B. Learning deconvolution network for semantic segmentation. In *Proceedings of the IEEE International Conference on Computer Vision*, 2015, pp. 1520–1528.

[29] Yu F, Koltun V. Multi-scale context aggregation by dilated convolutions. *arXiv preprint arXiv:1511.07122*, 2015.

[30] Boykov Y, Veksler O, Zabih R. Fast approximate energy minimization via graph cuts. *IEEE Transactions on pattern analysis and machine intelligence*, 2001, 23(11):1222–1239.

[31] He K, Zhang X, Ren S, Sun J. Delving deep into rectifiers: Surpassing human-level performance on imagenet classification. In *Proceedings of the IEEE International Conference on Computer Vision*, 2015, pp. 1026–1034.

[32] Jia Y, Shelhamer E, Donahue J, Karayev S, Long J, Girshick R, Guadarrama S, Darrell T. Caffe: Convolutional architecture for fast feature embedding. In *Proceedings of the 22nd ACM international conference on Multimedia*, 2014, pp. 675–678.

[33] Felzenszwalb P F, Huttenlocher D P. Efficient graph-based image segmentation. *International Journal of Computer Vision*, 2004, 59(2):167–181.

[34] Arbeláez P, Pont-Tuset J, Barron J T, Marques F, Malik J. Multiscale combinatorial grouping. In *Proceedings of the IEEE Conference on Computer Vision and Pattern Recognition*, 2014, pp. 328–335.

[35] Russakovsky O, Deng J, Su H, Krause J, Satheesh S, Ma S, Huang Z, Karpathy A, Khosla A, Bernstein M et al. Imagenet large scale visual recognition challenge. *International Journal of Computer Vision*, 2015, 115(3):211–252.

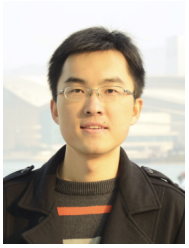

**Wei Zhang** is a Ph.D. candidate at the Department of Computer Science, The University of Hong Kong, Hong Kong. He received his B.E. degree in Automation college from Chongqing University in 2010 and M.S. degree in Institute of Pattern Recognition and Artificial Intelligence from Huazhong University of Science and Technology in 2013 respectively. His research interest covers image colorization and boundary detection.

**Chao-Wei Fang** is a Ph.D. candidate at the Department of Computer Science, The University of Hong Kong, Hong Kong. He received his B.E. degree in Automation from Xi'an Jiaotong University in 2013. His current research interests include image segmentation and image processing.

**Guan-Bin Li** received the PhD degree in computer science from the University of Hong Kong in 2016. He is currently a researcher in the school of Data and Computer Science, Sun Yat-sen University, China. He is a recipient of Hong Kong Postgraduate Fellowship. His current research interests include computer vision, image processing, and deep machine learning.

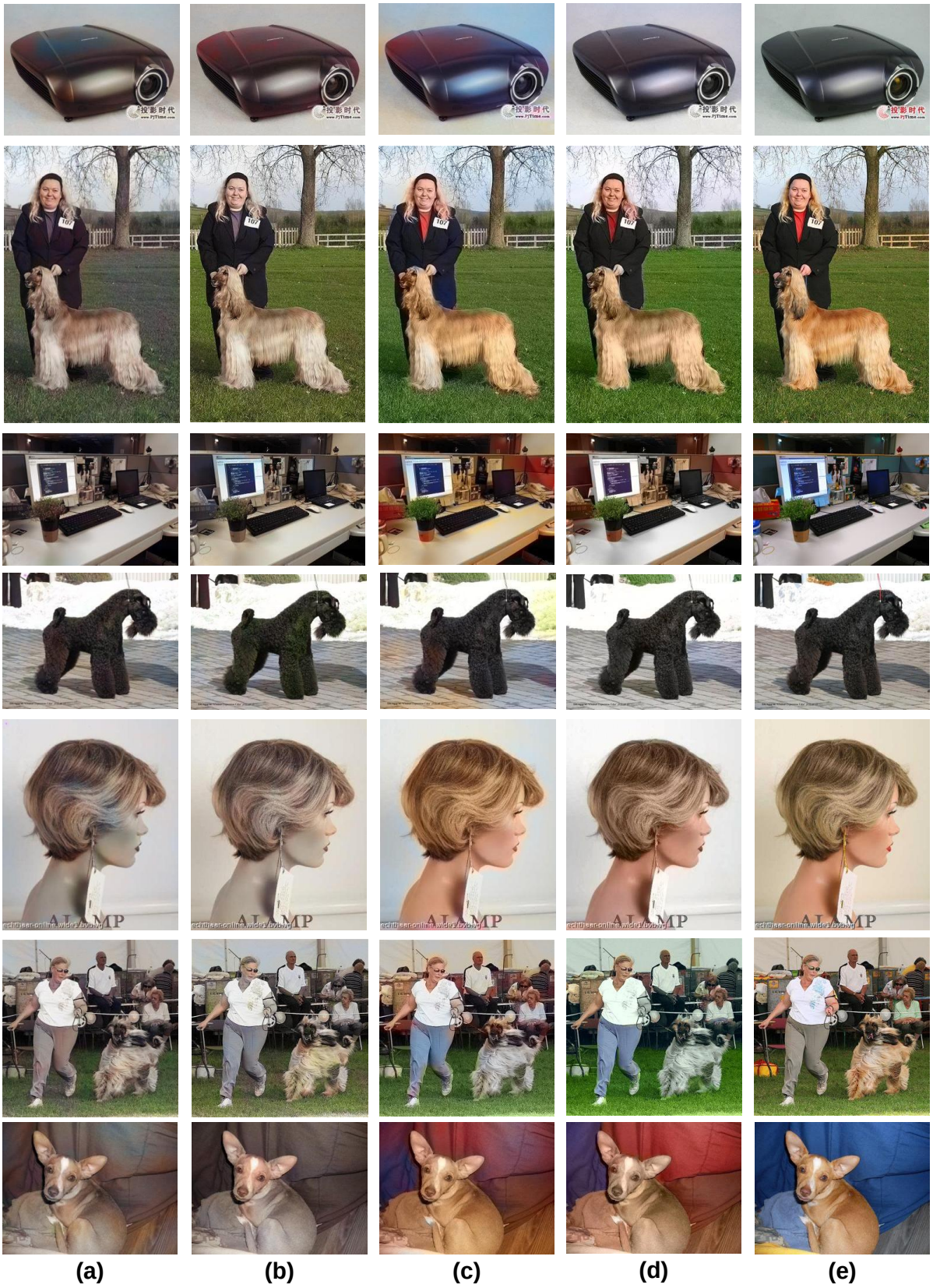


Fig. 9: Comparison with leading automatic colorization methods. *(a):* Dahl 2016 [17]; *(b):* Iizuka et al. [27]; *(c):* Richard et al. [19]; *(d):* Ours; *(e):* Ground-truth;


Fig. 10: Comparison with leading automatic colorization methods. *(a):* Grayscale input; *(b):* Dahl 2016; *(c):* Iizuka et al.; *(d):* Richard et al.; *(e):* Ours;